Advances in Coordination, Bioinorganic and Inorganic Chemistry
Edited by M. Melník, J. Šima, and M. Tatarko
Slovak Technical University Press, Bratislava © 2005

TUNABLE-FREQUENCY ELECTRON PARAMAGNETIC RESONANCE – A NOVEL TOOL TO INVESTIGATE HIGH-SPIN TRANSITION METAL COORDINATION COMPLEXES

J. Krzystek[a], A. Ozarowski[a], S. Trofimenko[b], S. A. Zvyagin[c] and J. Telser[d]

[a]*National High Magnetic Field Laboratory, Florida State University, Tallahassee, FL 32310, USA (e-mail: krzystek@fsu.edu)*
[b]*Department of Chemistry and Biochemistry, University of Delaware, Newark, DE 19716, USA*
[c]*Dresden High Magnetic Field Laboratory, Forschungszentrum Rossendorf, D-01314 Dresden, Germany*
[d]*Chemistry Program, Roosevelt University, Chicago, IL 60605, USA*

ABSTRACT

Although Electron Paramagnetic Resonance (EPR) has been a very successful method to investigate transition metal ions in coordination complexes and biomolecules, not all such ions can be subject to conventional EPR investigations even if they are paramagnetic. In particular, high-spin ($S > 1/2$) species pose serious challenges to spectroscopists, and of these, the non-Kramers (integer-spin) ions have been long considered 'EPR-silent' at conventional frequencies and fields.

We propose a novel EPR-related technique that takes an advantage of tunable sources operating in the sub-THz range of frequencies in conjunction with very high magnetic fields (up to 25 Tesla) to determine accurate intrinsic spin Hamiltonian parameters not only for a variety of non-Kramers transition metal ions (such as Ni^{2+}, Mn^{3+}, and Fe^{2+}) that have traditionally been termed 'EPR-silent', but also for those Kramers (half-integer) species that are poorly characterized in their high-spin states, such as Co^{2+}. The obtained parameters can serve to better characterize the electronic structure of the ions in question, in combination with other experimental methods.

INTRODUCTION

HFEPR [1] has become in the recent years an experimental method of choice in investigating a variety of spin systems that for various reasons can not be adequately characterized by conventional EPR [2]. The application of HFEPR to non-Kramers (integer-spin) paramagnetic species has been particularly compelling since many such systems cannot be characterized by EPR at conventional frequencies or magnetic fields primarily due to large zfs, often exceeding the microwave quantum energy of 0.3 cm^{-1} (X-band) or 1.2 cm^{-1} (Q-band) [3]. Typical examples of HS non-Kramers species investigated by HFEPR have been 3d transition metal ions since their zfs falls into the energy range conveniently obtainable by modern sub-THz source. Thus, such metal ions as V(III) ($3d^2$) [4], Mn(III) and Cr(II) (both $3d^4$) [5,6], Fe(II) ($3d^6$) [7] and Ni(II)($3d^8$) have been recently studied [8,9].

The methodology of extricating spin Hamiltonian parameters from HFEPR spectra has been initially the same as in conventional EPR: simulating the spectra using an initial set of spin Hamiltonian parameters, comparing the simulations with experiment, and adjusting simulation parameters in an iterative process until a satisfactory agreement was found. If – as is often the case – the sample is polycrystalline or contained in a glass, the simulation process involves constructing a powder pattern, averaging over all spatial orientations of the single crystal with respect of the magnetic field. In order to assure the adequacy of fitted spin Hamiltonian parameters, HFEPR experiments have been often performed at multiple frequencies [10]; however, the spin Hamiltonian parameters have usually been fitted to single-frequency spectra. More recently, spin Hamiltonian parameters have been fitted to a dataset obtained at a few discrete frequencies, usually obtained from the different harmonics of the Gunn oscillator source, which improved the fit accuracy [11].

It was noticed early on that polycrystalline transition metal complexes spectra often do not display characteristics of powder patterns. The reason is that the strong magnetic fields employed in HFEPR tend to align the crystallites with the direction of the largest magnetic susceptibility anisotropy parallel to the field. In certain cases the torquing effect is beneficial, resulting in quasi-single crystal spectra [12,13]. In most cases, however, the same effect is detrimental to spectral quality since it produces spectra that are neither ideally powder-patterned, nor single-crystal like, and renders them uninterpretable [14].

We propose that the best way around the above mentioned problems is an extension of the multifrequency HFEPR approach, which we call tunable-frequency HFEPR. This methodology dispenses with simulating single-frequency EPR spectra; instead, the frequency is tuned quasi-continuously, and resonances are plotted as a function of transition energy. The optimal spin Hamiltonian parameters are subsequently best-fitted to the complete two-dimensional dataset of experimental resonances [15], the fitting procedure being now fully automated. This methodology was borrowed from antiferromagnetic resonance, where particular AFMR modes are also traced in the two-dimensional field-frequency space [16,17]. In order to achieve maximum frequency tunability, and consequently the maximum number of experimental points, we have taken advantage of the availability of backward wave oscillator (BWO) tubes as sub-THz wave radiation sources, which had only rarely been employed in EPR [18,19]. In our application, four BWO tubes cover quasi-continuously the spectral range of 150—700 GHz (~5—23 cm^{-1}), although the range of BWOs in general is wider: ca. 24—1,300 GHz (~1—43 cm^{-1}) [20]. The quantum energy range of BWOs makes them an ideal tool for investigating transition metal complexes, since it covers the typical zfs values of those ions [3]. In this article we will show

how tunable-frequency methodology using BWOs facilitates recognition of HFEPR spectral features, and improves the accuracy of spin Hamiltonian parameters obtained from imperfect powder spectra. We will use as examples two non-Kramers ion complexes in their high-spin (paramagnetic) states: V(III) (d^2, S = 1) in $VBr_3(thf)_3$, where thf = tetrahydrofuran; and Fe(II) (d^6, S = 2) in the hexaaquaferrous ion $[Fe(H_2O)_6](II)$ as found in ferrous heptahydrate ($[Fe(H_2O)_6](SO_4) \bullet H_2O$, thereafter abbreviated as $FeSO_4$), and one Kramers ion: HS Co(II) ($3d^7$, S = 3/2) in $Co(PPh_3)_2Cl_2$ complex. The V(III) complex has been studied before by HFEPR using the multifrequency methodology based on Gunn oscillator sources [4]. The Co(II) complex was an object of a recent paper [22]. $FeSO_4$ has not been investigated by EPR to our best knowledge.

EXPERIMENTAL PART

Samples.

All HFEPR experiments were performed on ca. 20-40 mg of loose polycrystalline samples of the three complexes described above. The details of sample preparation are described in the referenced papers. In the case of $CoCl_2(PPh_3)_2$ some experiments were performed on a sample constrained in a KBr pellet, since that particular complex strongly torques in field. $FeSO_4$ required extensive grinding before the experiment. Constraining the crystallites in KBr was also required.

Apparatus and equipment.

EPR spectroscopy. HFEPR spectra were recorded using the new Mm and Sub-mm Spectroscopy Facility at the NHMFL [23]. Tunable frequencies in the 150—700 GHz range (~5—23 cm^{-1}) were provided by a set of four BWOs (Institute of General Physics, Moscow, Russian Federation). The high-voltage power supply and the permanent magnet housing for the tubes were acquired from the same source. The frequency was pre-calibrated using a Fabry-Perot resonator. The magnet used was the resistive "Keck" magnet (0—25 T) of improved homogeneity (12 ppm in 1 cm diameter spherical volume) and temporal stability. The field was pre-calibrated using an NMR probe, and was checked during the experiment using a DPPH marker. The oversized-pipes wave propagation system was home-built along the principles outlined before [24]. Detection was provided with an InSb hot-electron bolometer (QMC Ltd., Cardiff, UK). Modulation for detection purposes was provided alternatively by modulating the magnetic field (1 kHz frequency, 1 mT max. amplitude), or by chopping the sub-THz wave beam at ca. 300 Hz. A Stanford SR830 lock-in amplifier converted the modulated signal to DC voltage.

EPR analysis.

The magnetic properties of a high-spin species can be described by the standard spin Hamiltonian comprised of Zeeman and zfs terms [3]:

$$\mathrm{H} = \beta\, B \bullet \mathbf{g} \bullet S + D(S_z^2 - S(S+1)/3) + E(S_x^2 - S_y^2) \qquad (1a)$$

for $S \leq 3/2$ spin species, or

$$\mathrm{H} = \beta\, B \bullet \mathrm{g} \bullet S + D(S_z^2 - S(S+1)/3) + E(S_x^2 - S_y^2) + B_4^0 O_4^0 + B_4^2 O_4^2 + B_4^4 O_4^4 \qquad (1b)$$

for higher spin numbers. The hyperfine interactions, and higher-order Zeeman terms have been ignored.

The EPR resonances were collected as a function of sub-THz quantum energy and the resulting two-dimensional (field vs. energy) array was simultaneously fitted by use of a non-linear least squares (Simplex) method to minimize the function:

$$\chi^2 = \sum_{i=1}^{N} (f_i^{(calc)} - f_i^{(\exp)})^2 \qquad (2)$$

where f_i are the calculated and experimental resonance fields. The S = 1 resonances were calculated using the well-known formulas resulting from the exact solution of the secular equation [25]. The S = 3/2 and S = 2 resonance fields were calculated in an iterative procedure that employed the Householder method [26] to diagonalize the spin Hamiltonian in Eq. 1. The least-squares procedure was used to obtain best fit parameters for the entire field vs. energy array of EPR transitions. Errors in the parameters were estimated by use of the Hessian matrix method [27]. In single-frequency spectral simulations transition probabilities were calculated from the eigenvectors in a standard way [28], and the calculated transition intensities were corrected for the Boltzmann populations of the levels involved.

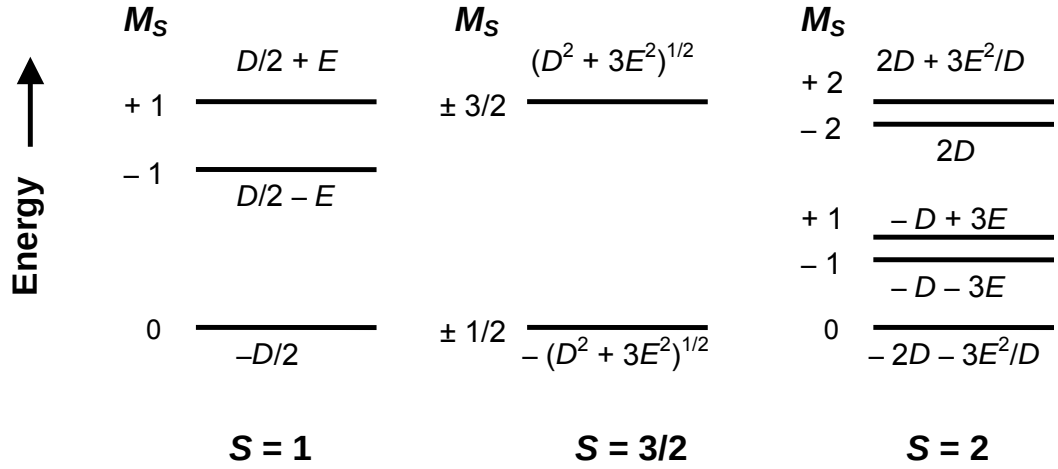

Chart 1. The result of second-order zero-field splitting terms of spin Hamiltonian (1) acting on spin wavefunctions corresponding to different spin multiplicities, for D and E > 0.

RESULTS AND DISCUSSION

$VBr_3(thf)_3$, S = 1. A single-frequency spectrum of polycrystalline $VBr_3(thf)_3$ is shown in Fig. 1.

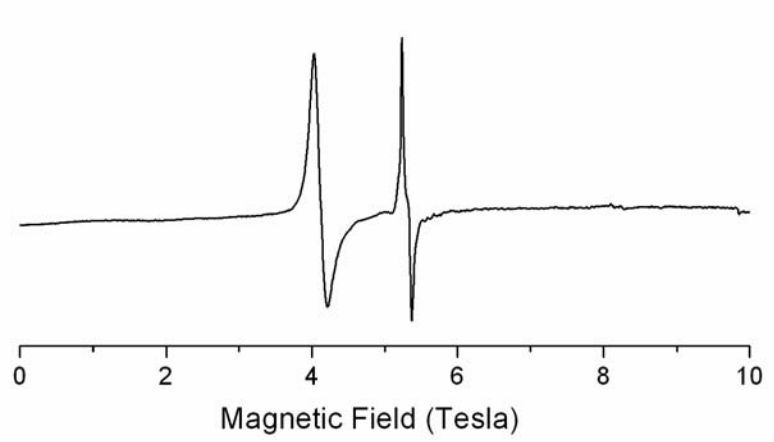

Fig. 1. An HFEPR spectrum of $VBr_3(thf)_3$ at 337 GHz and 10 K.

It is clear that the experimental spectrum does not correspond to an ideal random distribution of the crystallites in the sample, and is difficult to interpret qualitatively based on the known theory of triplet state EPR [25]. In this situation, obtaining fairly accurate values of the spin Hamiltonian parameters from the spectra was only possible through multi-frequency experiments using the multiple harmonics of the then available Gunn oscillator sources [4]. In the present work we employed tunable-frequency HFEPR to collect and plot the resonances in polycrystalline $VBr_3(thf)_3$, as a function of sub-THz wave energy. The field vs. quantum energy dependence of these resonances is shown in Fig. 2 as squares.

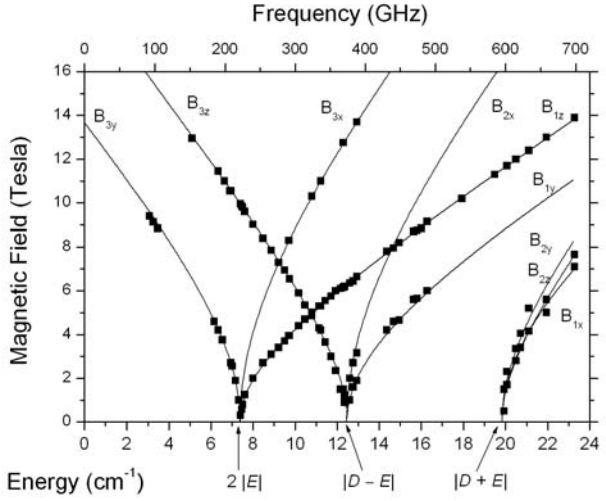

Fig. 2. Tunable-frequency HFEPR in an S = 1 spin system. Field vs. quantum energy dependence of EPR resonances in polycrystalline $VBr_3(thf)_3$ at 10 K. Three zero-field resonances at ca. 7.5, 12.5 and 20 cm^{-1} are observed directly and labeled accordingly. The squares are experimental HFEPR points while the curves were simulated using the following best-fit spin Hamiltonian parameters: S = 1, D = –16.162 cm^{-1}, E = –3.694 cm^{-1}, g_x = 1.86, g_y = 1.90, g_z = 1.71. The particular transition branches are identified using standard nomenclature for triplet states with rhombic symmetry.

The above plot immediately offers several hints as to the origin of the observed resonances, and gives an estimate of spin Hamiltonian parameters. First, it was possible to directly detect three zero-field resonances at ca. 7.5, 12.5 and 20 cm^{-1}. These can be identified as $2|E|$, $|D - E|$ and $|D + E|$ transitions (see Chart 1). From Fig. 2 it is also easy to differentiate between the allowed ($\Delta M_s = \pm 1$) and forbidden ($\Delta M_s = \pm 2$) transitions, since the latter have a much less steep slope than the former, corresponding to a higher effective g-value. The final identification of particular branches in the spectrum was achieved through simulations, which also finalized the spin Hamiltonian values as given in Table 1. Altogether, the fits yielded a remarkable agreement with the experiment, as witnessed by Fig. 2, and the small error values in spin Hamiltonian parameters as presented in Table 1.

$Co(PPh_3)_2Cl_2$, S = 3/2. A single-frequency spectrum of polycrystalline $Co(PPh_3)_2Cl_2$ is shown in Fig. 3 together with a simulation generated using spin Hamiltonian parameters as in Table 1.

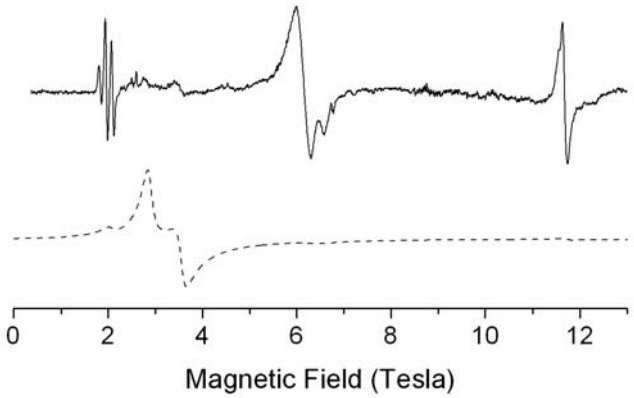

Fig. 3. Experimental (solid) and simulated (dashed) HFEPR spectrum of polycrystalline $Co(PPh_3)_2Cl_2$ at 190 GHz and 20 K. The simulation assuming powder pattern used following spin Hamiltonian parameters: S = 3/2, D = –14.76 cm^{-1}, E = –1.141 cm^{-1}, g_x = 2.166, g_y = 2.17, g_z = 2.240.

It is obvious that the experimental spectrum does not correspond to a powder pattern; in contrary, it suggests a strong alignment of the crystallites with field (torquing). The identification of the particular peaks in the $Co(PPh_3)_2Cl_2$ spectra was thus not possible based

on single-frequency experiments, and neither was the determination of the spin Hamiltonian parameters from them. We thus employed tunable-frequency HFEPR, and obtained a plot of all observed resonances as a function of sub-THz quantum energy, shown in Fig. 4 as squares.

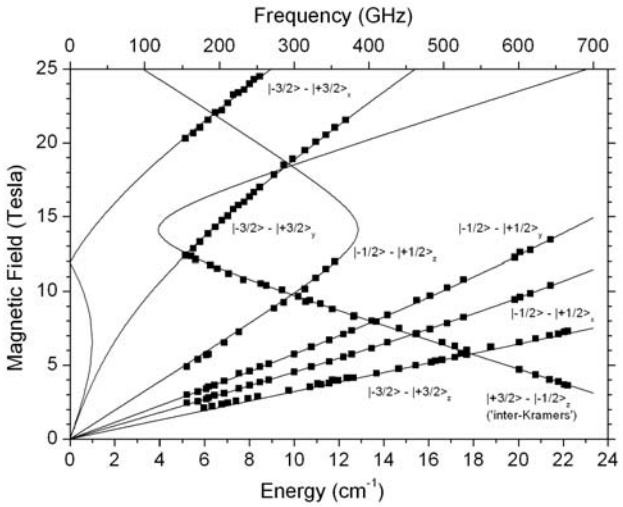

Fig. 4. Tunable-frequency HFEPR in an S = 3/2 spin system. Field vs. sub-THz quantum energy dependence of EPR resonances in polycrystalline $CoCl_2(PPh_3)_2$. Experimental resonance positions at specific frequencies are given by the squares. The single zero-field resonance lies outside the spectrometer range at ca. 30 cm^{-1}.The lines were calculated using the best-fitted spin Hamiltonian parameters as in Figure 3. Particular transition branches are identified and labeled accordingly.

The plot immediately identifies the parallel intra-Kramers transitions within the ±3/2 doublet (effective g ~ 6.6), and within the ±1/2 doublet (effective g ~ 2.2), both kinds of transitions originating from the zero energy point at zero field. In addition, the tunable-frequency experiment on a loose sample identified the inter-Kramers transition between the two doublets, which, when extrapolated to high energies, occurs at about 30 cm^{-1} at zero field. The 30 cm^{-1} value is thus a good estimate of zfs in this high-spin Co(II)complex, which for S = 3/2 is equal to $2|D|$ in an axial case, and $2(D^2 + 3E^2)^{1/2}$ in a rhombic case (see Chart 1). Constraining the crystallites in a KBr pellet did produce a powder pattern, agreeing with single-frequency simulations. The perpendicular peaks then visible originate from the excited intra-Kramers transition within the ±1/2 doublet. This observation gives a measure of the zfs parameter E, but not D. The experimental points obtained for the pellet were thus included in the complete dataset together with the loose-sample points, shown in Fig. 4. A simultaneous fit of spin Hamiltonian parameters to the two-dimensional experimental field-energy dataset (squares in Fig. 4) yielded a set of spin Hamiltonian parameters presented in Table 1. The quality of these parameters can be judged by the agreement of the calculated lines in Fig. 4

with the experimental resonances. Temperature-dependent single-frequency experiments unequivocally established the sign of *D* in this system as negative, i.e. the ±3/2 doublet lying lower on the energy scale than the ±1/2 doublet [22].

$FeSO_4$, S = 2. Compared to the previous two complexes, $FeSO_4$ is a particularly difficult system to work with, as are most Fe(II) complexes [7,29,30]. The main challenge from the experimental point of view is the tendency of the crystallites to congregate in high magnetic fields into discrete quasi-single crystals despite their being carefully ground prior to the experiment. This results in spectra corresponding neither to a single crystal, nor to a true powder, and renders them uninterpretable. Pressing the solid sample with KBr in a pellet only partly solved this problem, as shown in Figure 5. The other problem concerns spectral interpretation. As shown in Figure 5, the spectra are not particularly rich in recognizable features. A trial-and-error procedure to find the spin Hamiltonian parameters from single-frequency spectra proved therefore impractical.

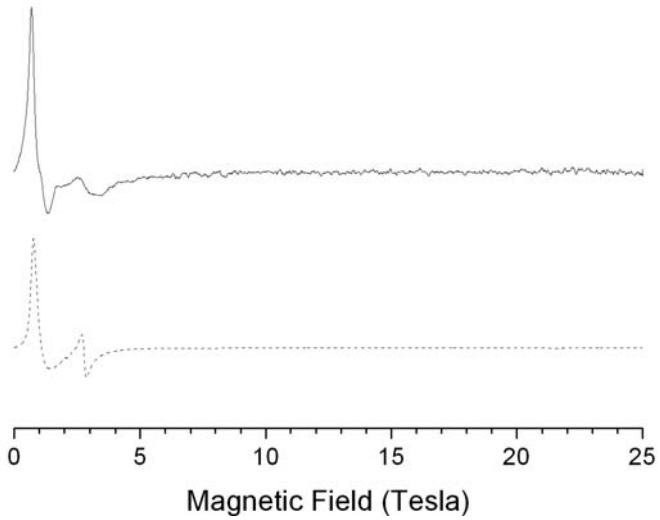

Fig. 5. HFEPR spectrum of a $FeSO_4$ pellet at 167 GHz and 4.2 K (top, solid) and its simulation (bottom, dashed line) using the following spin Hamiltonian parameters obtained from tunable-frequency experiment: D = +10.2 cm^{-1}, E = 2.24 cm^{-1}, g_x = 2.13, g_y = 2.20, g_z = 2.10.

The practical solution to problems encountered in $FeSO_4$ and outlined above was found in a tunable-frequency experiment. The complete two-dimensional field-energy dataset for this quintet spin species is presented in Fig. 6 as squares. The prominent feature of this plot is the presence of three zero-field resonances, appearing at ca. 5, 13.5 and 18.5 cm^{-1}. Since the low-frequency value (5 cm^{-1}) is approximately the difference of the two high frequencies (13.5 and 18.5 cm^{-1}), a possible initial assignment of the zf resonances is to attribute them to the 6E, (D – 3E), and (D + 3E) zf transitions, respectively (ignoring the

$3E^2/D$ factor in the case of low rhombicity, see Chart 1), similarly to the case of the perchlorate salt. This assignment results in the following values of the zfs parameters: D = 16 cm^{-1}; E = 0.83 cm^{-1}. However, an attempt to fit the field vs. energy resonances as shown in Figure 6 using these parameters was wholly unsuccessful. Instead, the following assignment of the three observed resonances: ($D - 3E + 3E^2/D$), ($6E$), ($D + 3E$) results in the values: D = 10.2, E = 2.24 cm^{-1} and an immediate agreement between the simulation and experiment, when using the following g-matrix values: g_x = 2.13, g_y = 2.20, g_z = 2.10. As this manuscript is being submitted, we have not yet subjected the data set to a computer fit, which will undoubtedly refine the spin Hamiltonian parameters. Therefore the above values, although close to optimal, are preliminary only, as visible from certain discrepancies between experiment and simulation in the field vs. energy plots shown in Figure 6. Also, fourth-order zfs parameters cannot be easily estimated without a computer fit.

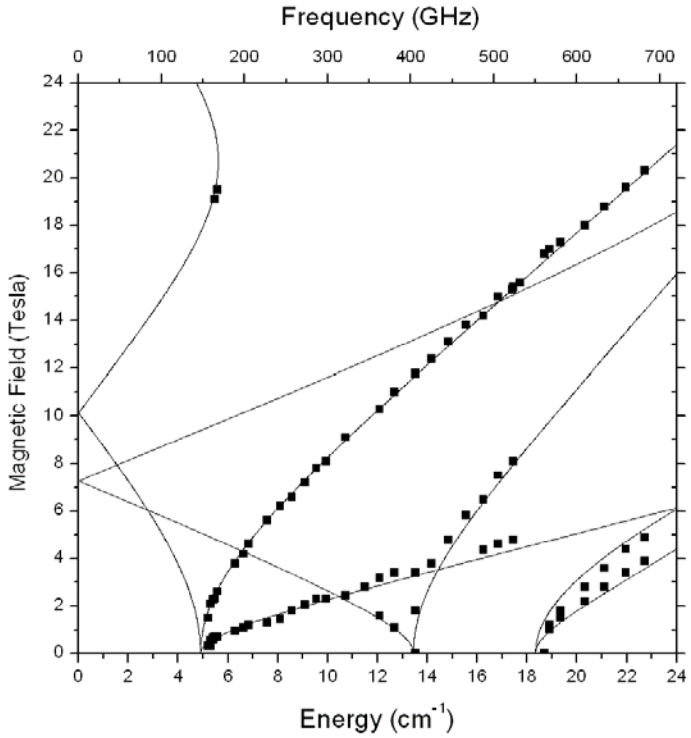

Fig. 6. Tunable-frequency HFEPR in an S = 2 spin system. Field vs. quantum energy dependence of EPR resonances in polycrystalline $FeSO_4$. Experimental resonance positions at specific frequencies are given by the squares. Three zero-field transitions are directly detected at ca. 5, 13.5 and 18.5 cm^{-1}. The lines were calculated using the following spin Hamiltonian parameters: D = +10.2 cm^{-1}, E = +2.24 cm^{-1}, g_x = 2.13, g_y = 2.20, g_z = 2.10.

Table 1. Spin Hamiltonian parameters for the three complexes investigated within this work.

Complex	S	D (cm^{-1})	E (cm^{-1})	g_x	g_y	g_z
$VBr_3(thf)_3$	1	–16.162(6)	–3.694(4) [a]	1.86(1)	1.90(1)	1.710(4)
$CoCl_2(PPh_3)_2$	3/2	–14.76(2)	–1.141(8)	2.166(4)	2.170(4)	2.240(5)
$FeSO_4$ [b]	2	+10.2	+2.24	2.13	2.20	2.10

[a] The sign of E was assumed identical to D in all cases.

[b] Spin Hamiltonian parameters for $FeSO_4$ have not yet been refined, so no errors are given.

Advantages and Disadvantages of Tunable-Frequency EPR.

We have introduced above a new methodological and experimental concept in the field of Electron Paramagnetic Resonance, which we call Tunable-Frequency EPR. This novel methodology is particularly amenable to investigating high-spin paramagnetic transition metal complexes. This is so for a variety of reasons that will be outlined below.

The phenomenon that appears in all high-spin systems is the zero-field splitting. This is the field-independent splitting of the M_s levels corresponding to the ground spin state through the admixture of higher-lying exciting states. This admixture is effected through the spin-orbit coupling, which can strongly vary from one system to another. As a result, high-spin transition metal complexes display a stunning variety of zfs magnitude, from very small, on the order of 10^{-2} cm^{-1} (Mn^{2+} in high-symmetry environment) to 10^{2} cm^{-1} (Co^{2+} in octahedral symmetry). If we discard the extreme cases, the range of 1—50 cm^{-1} is quite typical for high-spin transition metal ions. The use of tunable radiation sources operating in the sub-THz regime in combination with rapidly-swept magnetic fields assures that many if not most transitions between spin sublevels in these systems are spectrally covered. This is particularly important in non-Kramers metal ions, where the zero-field degeneracy within the particular $\pm M_S$ manifolds is lifted in zero-field conditions in the case of low symmetry. However, tunable-frequency EPR is very useful in the case of Kramers ions as well, since it enables us to observe transitions between different $\pm M_S$ manifolds, and thus allows to measure the magnitude and often also sign of the zfs parameters in ions such as Co^{2+}.

In principle, it should be possible to observe EPR resonances if the *single* operating frequency is higher than the magnitude of zfs splitting. While this is certainly true, there are several instances, presented above, where the spectra do not correspond to ideal powder pattern thus making the recognition of spectral features difficult or impossible. The application of tunable frequency usually facilitates the recognition of these features. Most importantly, it offers a unique opportunity to tune in to zero-field resonances, thus measuring directly the zfs parameters in the absence of field. Applying (high) magnetic field subsequently verifies the attribution of zf resonances in complicated spin systems (such as the quintet, or higher-multiplicity states), and allows to refine the zfs parameters values. Finally, applying magnetic field serves to establish the g-matrix values, thus completing the process of extracting complete spin Hamiltonian parameter set from the HFEPR spectra.

Tunable-frequency EPR is not free of disadvantages, compared to single-frequency experiments. One of the most important ones is a relatively low sensitivity. The reasons for it were discussed in a previous paper [21] and remain beyond the scope of this work. In brief, single-frequency spectrometers can be optimized to perform at a specific frequency, while

a tunable-frequency instrument needs to have a possibly broadband response at the expense of sensitivity. This has a negative impact on investigating samples with low spin concentrations, notably metalloproteins. Nevertheless tunable-frequency EPR is perfectly suited for measuring simple coordination complexes, some of which serve as biomimicking models for the more complicated biomolecules.

Finally, we will touch on the importance of the results obtained in this work. Vanadium(III) is an infrequent valence state of this element and as such of mostly academic interest. However, its presence was postulated in marine organisms [31] called tunicates [32]. Also, it was shown to inhibit insulin [33]. Of particular relevance here is the recent use of V(III) complexes as building blocks for single molecule magnets [34] and the synthesis of novel layered materials that contain V(III) [35-37].

Cobalt(II) tends to replace „spectroscopically-silent" zinc in a variety of proteins [38]. It consequently ends up in the high spin state, which although detectable by conventional EPR, cannot be adequately characterized using low frequencies and magnetic fields. The work described here was the first definitive determination of the zfs in tetrahedral high-spin Co(II) complexes [22]. Its continuation in a series of related tetrahedral complexes is currently in progress.

Finally, the role of iron in biochemistry cannot be underestimated. Of several valence states of this element, Fe(II) has been the most elusive from the point of EPR, and often termed „EPR-silent". Although some Fe(II) complexes have been characterized recently using HFEPR [7,29,30], the current work is the first ever on this most simple of Fe(II) complexes, namely the hexaaqua ion.

The importance of the reported EPR work is that spin Hamiltonian parameters obtained from EPR help deliver, in conjunction with other experimental methods, essential information on the electronic structure of the metal ion in question, which in turn is of importance to understanding its function, for example as catalysts in chemistry or biochemistry.

Acknowledgements. NHMFL is funded by the National Science Foundation through Cooperative Agreement DMR 0084173, and the State of Florida. The W. M. Keck Foundation, Los Angeles, funded the high-homogeneity 25-Tesla resistive magnet.

REFERENCES

1. Abbreviations used: BWO, backward wave oscillator; EPR, electron paramagnetic resonance; HFEPR, high-frequency and -field EPR; HS, high-spin; zf, zero-field; zfs, zf splitting.
2. P. C. Riedi and G. M. Smith, in B. C. Gilbert, M. J. Davies, D. M. Murphy (Eds.), Electron Paramagnetic Resonance. Royal Society of Chemistry, Cambridge, UK, 2002, p. 254.
3. A. Abragam and B. Bleaney: Electron Paramagnetic Resonance of Transition Ions, Dover Publications, Inc., New York, 1986.
4. J. Krzystek, A. T. Fiedler, J. J. Sokol, A. Ozarowski, S. A. Zvyagin, T. C. Brunold, J. R. Long, L.-C. Brunel, and J. Telser, Inorg. Chem. 43 (2004) 5645.
5. A.-L. Barra, D. Gatteschi, R. Sessoli, G. L. Abbati, A. Cornia, A. C. Fabretti, and M. G. Uytterhoeven, Angew. Chem. Intl. Ed. 36 (1997) 2329.
6. J. Krzystek, J. Telser, L. A. Pardi, D. P. Goldberg, B. M. Hoffman, and L.-C. Brunel, Inorg. Chem. 38 (1999) 6121.
7. M. J. Knapp, J. Krzystek, L.-C. Brunel, and D. N. Hendrickson, Inorg. Chem. 39 (2000) 281.
8. L. A. Pardi, A. K. Hassan, F. B. Hulsbergen, J. Reedijk, A. L. Spek, and L.-C. Brunel, Inorg. Chem. 39 (2000) 159.
9. J. Krzystek, J.-H. Park, M. W. Meisel, M. A. Hitchman, H. Stratemeier, L.-C. Brunel, and J. Telser, Inorg. Chem. 41 (2002) 4478.
10. P. J. M. van Kan, E. van der Horst, E. J. Reijerse, P. J. M. van Bentum, and W. R. Hagen, Journal of the Chemical Society, Faraday Transactions 94 (1998) 2975.
11. P. L. W. Tregenna-Piggott, H. Weihe, and A.-L. Barra, Inorg. Chem. 42 (2003) 8504
12. A. L. Barra, A. Caneschi, D. Gatteschi, and R. Sessoli, J. Am. Chem. Soc. 117 (1995) 8855.
13. D. P. Goldberg, J. Telser, J. Krzystek, A. G. Montalban, L.-C. Brunel, A. G. M. Barrett, and B. M. Hoffman, J. Am. Chem. Soc. 119 (1997) 8722.
14. J. Krzystek, G. Yeagle, J.-H. Park, M. W. Meisel, R. D. Britt, L.-C. Brunel, and J. Telser, Inorg. Chem. 42 (2003) 4610.
15. L. A. Pardi, J. Krzystek, J. Telser, and L.-C. Brunel, J. Magn. Reson. 146 (2000) 375.
16. G. E. Fanucci, J. Krzystek, M. W. Meisel, L.-C. Brunel, and D. R. Talham, J. Am. Chem. Soc. 120 (1998) 5469.

17. K. Katsumata, J. Phys.: Condens. Matter 12 (2000) R589.
18. Y. Alpert, J. Couder, J. Tuchendler, and H. Thome, Biochim. Biophys. Acta 332 (1973) 34.
19. V. F. Tarasov, G. S. Shakurov, B. Z. Malkin, and V. A. Ulanov, in C. Z. Rudowicz (Ed.), Modern applications of EPR/ESR. Springer, Singapore, 1998.
20. G. Kozlov and A. Volkov, in G. Grüner (Ed.), Topics in Applied Physics: Millimeter and Submillimeter Wave Spectroscopy of Solids. Springer, Berlin, 1998, p. 51.
21. J. Krzystek and J. Telser, J. Magn. Reson. 162 (2003) 454.
22. J. Krzystek, S. A. Zvyagin, A. Ozarowski, A. T. Fiedler, T. C. Brunold, and J. Telser, J. Am. Chem. Soc. 126 (2004) 2148.
23. S. A. Zvyagin, J. Krzystek, P. H. M. van Loosdrecht, G. Dhalenne, and A. Revcolevschi, Phys. Rev. B 67 (2003) 212403.
24. A. K. Hassan, L. A. Pardi, J. Krzystek, A. Sienkiewicz, P. Goy, M. Rohrer, and L.-C. Brunel, J. Magn. Reson. 142 (2000) 300.
25. P. Kottis and R. Lefebvre, J. Chem. Phys. 41 (1964) 379.
26. J. H. Wilkinson: The Algebraic Eigenvalue Problem, Clarendon Press, London, 1970.
27. W. H. Press, B. P. Flannery, A. A. Teukolsky, and W. T. Vetterling, Numerical Recipes in Pascal. Cambridge University Press, Cambridge, 1989, p. 572.
28. A. Bencini and D. Gatteschi, in G. A. Melson, B. N. Figgis (Eds.), Transition Metal Chemistry. Marcel Dekker, New York, 1982, p. 1.
29. G. Carver, P. L. W. Tregenna-Piggott, A.-L. Barra, A. Neels, and J. A. Stride, Inorganic Chemistry 42 (2003) 5771
30. A. Ozarowski, S. A. Zvyagin, W. M. Reiff, J. Telser, L. C. Brunel, and J. Krzystek, J. Am. Chem. Soc. 126 (2004) 6574.
31. W. C. A. Wilisch, M. J. Scott, and W. H. Armstrong, Inorg. Chem. 27 (1988) 4333.
32. K. Kustin, W. E. Robinson, R. B. Frankel, and K. Spartalian, J. Inorg. Biochem. 63 (1996) 223.
33. M. Melchior, S. J. Rettig, B. D. Liboiron, K. H. Thompson, V. G. Yuen, J. H. McNeill, and C. Orvig, Inorg. Chem. 40 (2001) 4686.
34. S. L. Castro, Z. Sun, C. M. Grant, J. C. Bollinger, D. N. Hendrickson, and G. Christou, J. Am. Chem. Soc. 120 (1998) 2365.
35. D. Grohol, D. Papoutsakis, and D. G. Nocera, Angew. Chem. Int. Ed. 40 (2001) 1519.

36. D. Grohol and D. G. Nocera, J. Am. Chem. Soc. 124 (2002) 2640.

37. D. Papoutsakis, D. Grohol, and D. G. Nocera, J. Am. Chem. Soc. 124 (2002) 2647.

38. W. Maret and B. L. Vallee, Methods Enzymol. 226 (1993) 52.